Letters in Applied NanoBioScience
Open-Access Journal (ISSN: 2284-6808)

Article
Volume 13, Issue 4, 2024, 177
https://doi.org/10.33263/LIANBS134.177

Synthesis, Anti-oxidant and Cytotoxicity Activity of ZnO Nanoparticles Wrapped with *Citrus aurantium*

Nasser Mohammed Hosny [1,*], Amr S. Eissa [1], Amira A. Awadalla [2], Lamiaa A. A. Barakat [1]

[1] Chemistry Department, Faculty of Science, Port Said University, POB 42522 Port Said, Egypt
[2] Center of Excellence for Genome and Cancer Research, Urology and Nephrology Center, Mansoura University, Mansoura 35516, Egypt
* Correspondence: nasserh56@yahoo.com;

Scopus Author ID 55893672800
Received: 22.08.2023; Accepted: 8.07.2024; Published: 27.08.2024

Abstract: ZnO and *Citrus aurantium* oil (CA) have promising cytotoxicities against various cell lines. The manuscript aimed to synthesize, characterize, and study the antioxidant and cytotoxicity activity of ZnO coated with *Citrus aurantium*. ZnO nanoparticles were synthesized and modified by *Citrus aurantium* (CA). Infrared spectra (FT-IR), ultraviolet and visible spectra (UV-Vis.), X-ray powder diffraction (XRD), transmittance electron microscope (TEM), selected area electron diffraction (SAED), and high-resolution transmittance electron microscope (HRTEM). The formation of hexagonal ZnO nanoparticles with an average crystallite size of 13 nm was approved by XRD, TEM, HRTEM, and SAED. *Citrus aurantium* was loaded onto ZnO nanoparticles, forming rod-like crystals with an average particle size of 34 nm. The optical band gaps were determined and found to be 3.4 and 3.7 eV; for ZnO NPs and ZnO wrapped with (CA), respectively. The cytotoxicity of (CA) and ZnO NPs loaded with (CA) were investigated against HCT-116 and HePG-2 cell lines and exhibited IC50 values of 47.79 and 32.56 µg/ml, respectively. ZnO NPs loaded with (CA) exhibited 72 % scavenging activity against free radicals. ZnO loaded with *Citrus aurantium* (CA) showed higher cytotoxicity and anti-oxidant activity than *Citrus aurantium* and free ZnO nanoparticles.

Keywords: zinc oxide nanoparticles; *Citrus aurantium*; cytotoxicity; anti-oxidant.

1. Introduction

Cancer is one of the chief causes of death worldwide. The number of cases of cancer is expected to reach 29.5 million by 2040 [1]. The most commonly used treatments for cancer are chemotherapy, surgery, and radiation, although their serious adverse effects are hair loss, diarrhea, vomiting, fever, and others [2].

Bioflavonoids are used in alternative medicine as antioxidants. They are found in the rind of citrus fruits. Bioflavonoids can control several biological processes, such as carcinogenesis and inflammatory and heart diseases. They have a protective effect on DNA against hydroxyl free radicals [3]. Moreover, the effects of flavonoids on the cell cycle and their ability to prevent the development of some cancer cell lines have been studied.

ZnO nanoparticles have gained much more attention in recent years as promising bioactive nanoparticles because of their biological and biomedical applications [4]. In addition to that, zinc oxide nanoparticles offer a wide range of applications, such as anticancer, antibacterial drugs, and gene delivery [5-11]. One of the most important advantages of ZnO is that it is administrated by the FDA (Food and Drug Administration) [12]. Because of its non-toxicity, biocompatibility, and antibacterial activity, ZnO is applied to treat skin disorders, such

as burns and irritations [13]. In addition to that, zinc oxide is inexpensive, widely accessible, and can be prepared in a variety of morphological forms.

Nano-structures of ZnO have been developed to increase their contact with the skin and the performance of the goods that are already on the market. Due to their unique physical and chemical characteristics, zinc oxide is one of the most significant metal oxides [14]. ZnO NPs have a variety of applications, including bioimaging, drug delivery, diabetes therapy, anti-inflammation, wound healing, and anti-cancer [15,16].

In addition to that, ZnO is thought to be non-toxic so it can be chosen as a biocompatible and biodegradable material based on these benefits. The anticancer activity of ZnO was investigated by several reports [17-19].

The risk of using ZnO comes from its ability to cause hepatic, pulmonary, and reproductive toxicity. The toxicity of it comes from the oxidative stress and genotoxicity [20].

Developing green drugs of natural ingredients is an essential demand among biologically active natural products [21-23]. One of the promising natural products is *Citrus aurantium* L, as it contains a variety of active bioflavonoids, such as rutin, neohesperidin, hesperidin, and naringin, which have antiviral and anticancer effects. Other ingredients, such as as tyramine, synephrine, octopamine, and N-methyltyramine, are present in *Citrus aurantium* juice. The *Citrus aurantium* provides ephedra benefits as the extract is rich in synephrine with its antidepressant properties [24-26]. The antiproliferative effect of *Citrus aurantium* stem on several cancer cell lines has been studied, and it has been found to have strong cytotoxicities against the tested cell lines [27].

To our knowledge, no work has been carried out on ZnO loaded with *Citrus aurantium* oil, which showed higher cytotoxicity than a free ZnO prepared previously [28].

This study describes the synthesis and characterization of ZnO nanoparticles loaded by CA. As ZnO and CA are anticancer agents, ZnO activity is expected to be enhanced after loading CA. To achieve this goal, the cytotoxicity and antioxidants of ZnO nanoparticles loaded with CA were investigated against HePG-2 and HCT-116.

2. Materials and Methods

2.1. Chemicals.

Zinc acetate dehydrate (99%) was purchased from Oxford Lab Fine Chem LLP. NaOH pellets (99.8 %) were procured from a local supplier. *Citrus aurantium* oil (CAO) natural, cold-compressed, California-origin, FG was supplied by Sigma-Aldrich, CAS NO.: 8008-57-9). The reagents used for bioassay and Doxorubicin are from (Sigma-Aldrich, St. Louis, MO., USA), and Fetal Bovine serum (GIBCO, UK).

2.2. Synthesis of ZnO and ZnO loaded CA.

A solution of 2.2 g of $Zn(OAc)_2.2H_2O$ in 100 mL distilled water and 0.4 g of NaOH in 30 mL distilled water were prepared. Sodium hydroxide solution was added slowly to $Zn(OAc)_2$. $2H_2O$ solution at 60°C with vigorous stirring for 12 hours. The mixture was cooled to room temperature, and the precipitate was isolated by centrifuging at 10000 rpm for 1/2 hr. The formed zinc oxide was washed with distilled water and dried at 60°C.

A measured volume (1 mL) of CA was added to the above-described reaction mixture to load CA and mediate the synthesis of ZnO. A yellow powder was formed after drying the product.

2.3. Cytotoxicity assay.

Cell lines HePG-2 and HCT-116, are two human tumors from VACSERA. Fetal bovine serum at a concentration of 10% was added to RPMI-1640 medium for their culture. 100 units/mL of penicillin and 100 g/mL of streptomycin were introduced as antibiotics at 37°C and in an incubator with 5% CO_2. As a standard anticancer drug, Doxorubicin was employed [29, 30].

MTT test was used to evaluate the inhibitory effects of ZnO loaded by CAO on the cell proliferation. The assay depends on living cells' succinate dehydrogenase of mitochondria to change tetrazolium bromide (MTT) (yellow color) of formazan (purple color). The cell RPMI-1540 was used as a medium to culture the cell, and fetal bovine serum (10%) was used as a medium. Additionally, antibiotics (100 g mL^{-1} of streptomycin +100 units/mL of penicillin) were added at 37°C. They are all incubated for 48 hours at 37°C and 5% CO_2. The cells were treated with different concentrations of ZnO-loaded CAO and kept in the incubator for 24 hours. 20 µL (5.0 mg/mL) MTT was added. 100 µL of DMSO was added, causing dissolving the color of formazan. The solutions were measured at 570 nm spectrophotometry by a plate reader (EXL 800, USA).

$$\%\ of\ Relative\ viability\ = \frac{Absorbance\ of\ treated\ sample}{Absorbance\ of\ untreated\ sample} \times 100 \quad (1)$$

2.4. Antioxidant activity.

The antioxidant activity was determined by 1,1-Diphenyl-2 picrylhydrazyl (DPPH). The antioxidant donates an electron to the DPPH radical, leading to decay in color. The change in the absorbance is measured at 520 nm. The tested samples were prepared from 140 µL of (1 mM) DPPH + 2.5 ml of 1:1 methanol along with 2, 4, 6, and 8 mg of ZnO-loaded CAO. The mixture was incubated for 1/2 hr at 37°C, and the absorbance was measured at 520 nm against a blank of 50% methanol. The IC_{50} value was calculated using the actual absorbance (ΔA) [31, 32].

$$\Delta A = The\ absorbance\ of\ the\ tested\ sample - The\ absorbance\ of\ the\ control \quad (2)$$

2.5. Instruments/characterization techniques.

FT-IR measurements were performed as potassium bromide disks on Nicolet iS50 FTIR (Thermo Fisher Scientific, USA) Spectrometer. For each interferogram, 16 scans were accumulated at a resolution of 4 cm^{-1}, and the samples were scanned in the region 4000–525 cm^{-1}. The results obtained were treated using Omnic software 9 V9.5. X-ray diffraction. To confirm the formation of ZnO NPs of the synthesized particles, X-ray diffraction (XRD) was done on a Shimadzu 6000 instrument (Cu Kα radiation 40 kV, 30 mA). Transmittance electron microscope (TEM) images were taken to characterize the morphology of the ZnO-loaded CAO samples Images by a JEOL 2100 Plus instrument operated at 200kV. UV–Vis absorption spectra were done by a spectrophotometer (JASCOUV-Vis Spectrophotometer - V630, Japan). Quartz Cells with a path length of 10 mm were used, and the samples were scanned in the 200-900 nm range.

3. Results and Discussion

A simple method was used to synthesize ZnO NPs, and *Citrus aurantium* oil (CAO) was loaded onto the formed ZnO nanoparticles. The synthesized products were characterized by various spectroscopic techniques.

3.1. FT-IR spectra.

FT-IR spectra were carried out to confirm the loading of *Citrus aurantium* onto ZnO (CA) (Figure. 1).

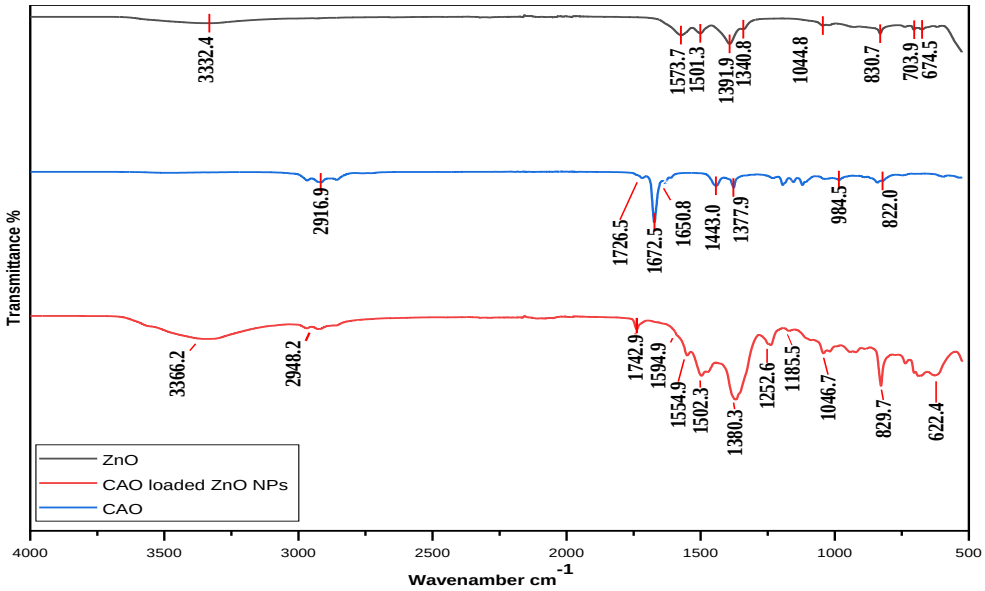

Figure 1. IR spectra of ZnO, ZnO loaded with CA and CA.

IR is an effective instrument for determining the functional groups present in the compounds. The spectrum of the pure CA shows characteristic peaks at 3479 cm^{-1}, which can be attributed to the (O-H) group of phenolic or enolic compounds [33, 34]. The bands in the region 2915-2967 cm^{-1} may be attributed to the stretching vibrations of N-H and C-H groups. These bands also exist in the spectrum of ZnO loaded with CAO, indicating loading the oil. The bands at 1726 cm^{-1} can be attributed to the asymmetric stretching vibrations of a protonated (COOH) group of free acids [35]. This band is shifted to a higher wavenumber in the spectrum of ZnO loaded with CAO owing to the participation of this group in coordination with ZnO. Besides that, the band at 1380 cm^{-1}, due to the symmetric stretching vibrations of the COOH group, is slightly shifted by 3.0 cm^{-1} and became more intense, thus supporting the suggestion of participation of this group in bonding [35].

The 1672 and 1632 cm–1 bands may be attributed to amidic (CONH) and in-plan–bending NH_2 groups, respectively [36]. The bands at 624 and 674 cm^{-1} are characteristic of ZnO [37]. The presence of the above bands suggests the formation of ZnO oxide loaded with *Citrus aurantium* oil.

3.2. XRD

XRD patterns of ZnO alone and ZnO loaded with CA are indicated in Figure. 2. The diffraction pattern of ZnO alone shows several peaks at 2θ = 31.7°, 34.3°, 36.1°, 47.4°, 52.6°, 59.5 and 61.8° corresponds to the planes (100), (002), (101), (102), (110), (103) and (200) which are indexed to ZnO (JCPDS card NO. 01-075- 0576). ZnO crystallizes as a hexagonal

crystal system with lattice parameters, a = b = 3.24 Å, c = 5.19 Å, α = β = 90° and ɣ = 120°. The diffraction pattern ZnO loaded with CAO shows a reduction in the intensity and slight shifts of some diffraction peaks compared with ZnO alone as a result of loading *Citrus aurantium*.

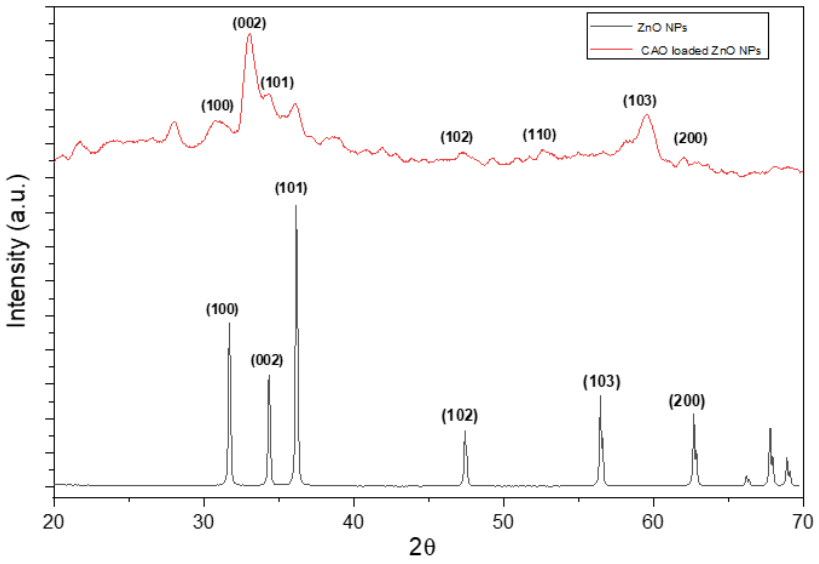

Figure 2. XRD patterns of ZnO alone and ZnO loaded with CA.

The crystallite sizes were determined for ZnO alone and ZnO loaded with CAO by applying the Scherer formula: $D = \frac{0.89\times \lambda}{\beta \cos\theta}$ (3) [38] (D is the crystallite size, λ is the wavelength of the x-rays = 0.15406 Å, β is the full wave at half maximum, can be calculated from the experimental peak width (FWHM). It has been corrected by subtracting the device broadening effect.

The crystallite sizes are 15.0 and 29 nm for ZnO and ZnO loaded with CAO, respectively. The crystallite size has increased in ZnO loaded with CAO due to the coating and the encapsulation of ZnO by CAO.

3.3. TEM and SAED.

TEM images of ZnO alone and ZnO-loaded CAO (Figure. 3) show that the particles of ZnO alone are irregular aggregated spheres. On the other hand, ZnO is loaded with CAO crystalline material with a hexagonal structure. The contrast in the images indicates the presence of two phases of ZnO and CAO. CAO coats the crystals of ZnO nanoparticles, forming an envelope around them.

The particles size distribution histogram (Figure. 4) of ZnO alone indicates that the particles are arranged in a narrow range from 5 to 25 nm with a maximum of 12 nm.

On the other hand, the particle size distribution histogram of ZnO loaded with CAO indicates the formation of particles with size in the range of 15-80 nm with a maximum of 34 nm. The relatively increment in the size of ZnO after loading CAO, comes from the formed layer of CAO around ZnO nanoparticles.

Selected area electron diffractions (SAED) and HRTEM of ZnO alone (Figure. 5) are used to support the formation of ZnO nanoparticles further. SAED pattern consists of several diffraction rings with the same center but different radii. The rings show the polycrystallinity of the sample.

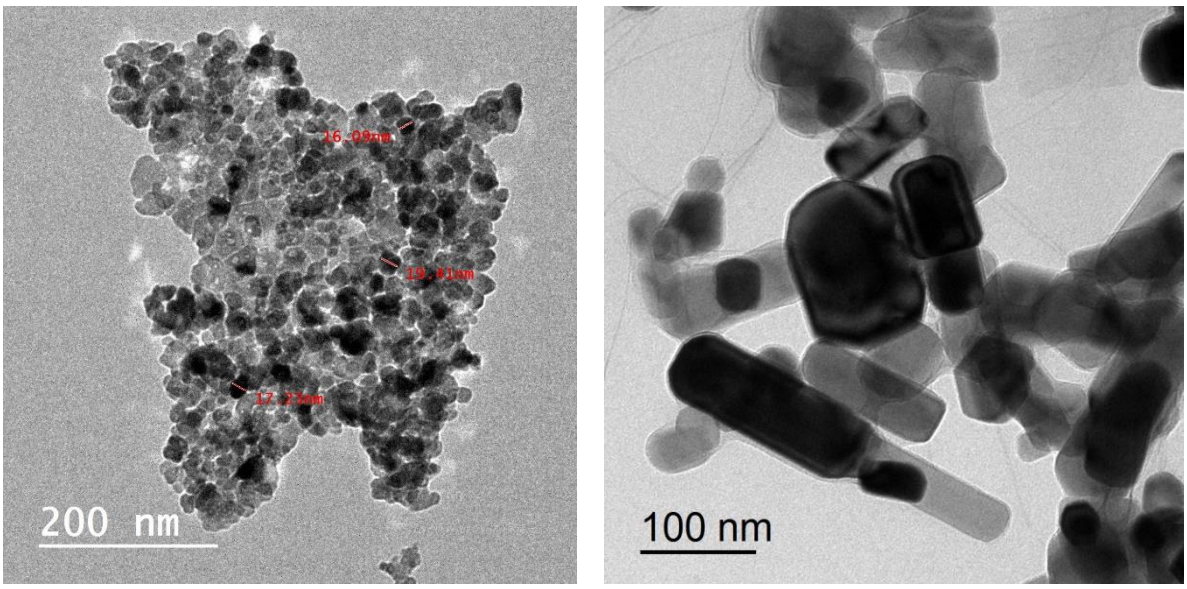

(a) **(b)**

Figure 3. TEM images **(a)** ZnO nanoparticles; **(b)** ZnO loaded with CAO.

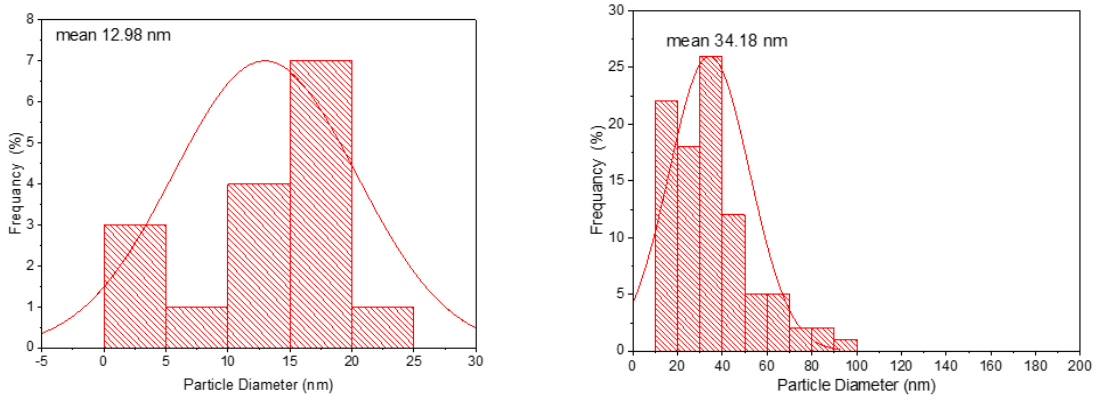

(a) **(b)**

Figure 4. Particle size distribution histograms of **(a)** ZnO alone; **(b)** ZnO loaded with CAO.

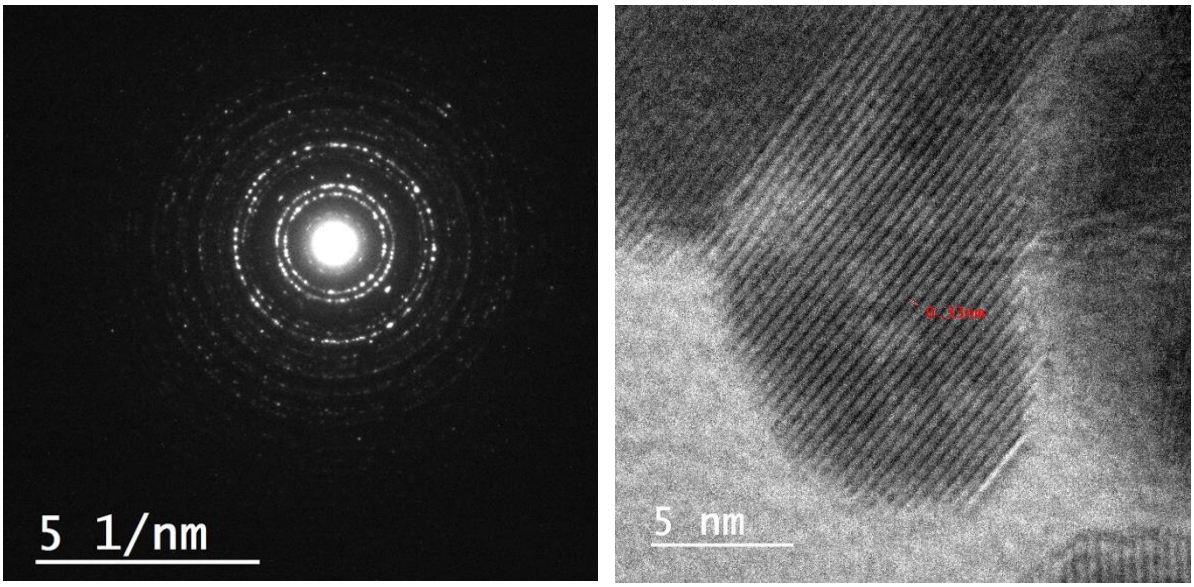

(a) **(b)**

Figure 5. (a) SAED; **(b)** HRTEM of ZnO nanoparticles.

The rings from inside to outside represent the planes (100), (002), (101), (102), (110), and (103), respectively. SAED is in good agreement with XRD and corroborates the formation of ZnO. HR-TEM study of ZnO shows lattice fringes well indexed with (100) plane of ZnO crystal lattice with d-spacing 0.3 nm.

3.4. UV–visible spectra.

UV-visible spectral analysis was employed to support the formation of zinc oxide. In the UV-visible spectra of ZnO NPs and ZnO loaded with CA (Figure 6), a band is observed at 359 nm due to the characteristic surface Plasmon band of ZnO NPs. Similar observations were obtained from previous reports, in which this characteristic band appears in the range from 310 to 380 nm [39,40]. There is a relationship between the absorption band position of ZnONPs caused by the surface Plasmon resonance and their sizes. This fact suggests that the redshift occurs when the size of nanoparticles increases and the energy decreases [41]. The presence of the surface plasmon band suggests the formation of ZnO NP. This band was observed at 316 nm on loading ZnO by CA as a result of overlapping the surface Plasmon with the several function groups of the organic oil that can absorb UV radiations due to $\pi \rightarrow \pi^*$ and $n \rightarrow \pi^*$ transitions.

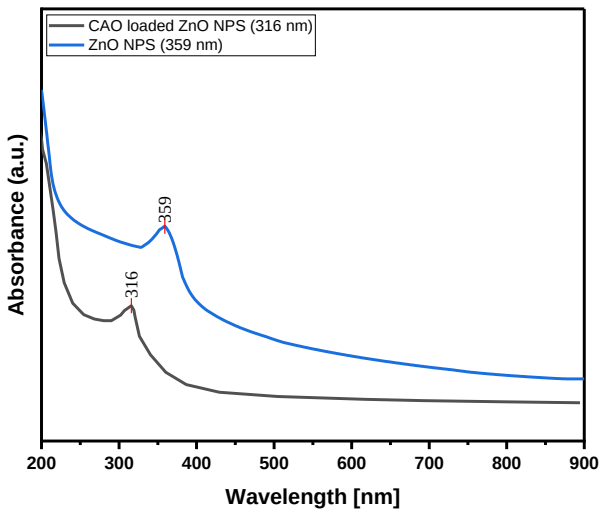

Figure 6. UV spectra of ZnO and ZnO loaded CAO.

The optical band gap (E_g), which is the energy difference between the conduction and the valence bands, was determined from UV spectra of ZnO and ZnO loaded CAO from Tauc's relation; the band gap energies (Figure. 7) were determined and compared with the bulk (3.3 eV). The determined bandgaps are 3.4 eV for ZnO NPs and 3.7 eV for ZnO loaded by CAO [42]. It is clear that the Eg of ZnO NPs alone is wider than the bulk due to the nanoscale size effects of ZnO; as the particle size is reduced, the band gap energy increases, as has been indicated previously [43-45]. ZnO-loaded CA has a wider band gap than pure ZnO NPs alone due to the interaction of the organic constituents of CA with the orbitals of ZnO NPs.

3.5. Cytotoxicity assay.

This research tried to shed some light on CA as a potential natural anticancer chemotherapeutic agent. The MTT assay was used to assess the cytotoxic activity and the IC_{50} value, as shown in Table 1 and Figure. 8. The cytotoxic effects of Doxorubicin, ZnO-loaded CA, and CA against HePG-2 and HCT-116 were investigated. The results showed that CAO

has moderate activity against HePG-2 and HCT-116 cell lines, while ZnO-loaded CA showed better activity against both HePG-2 and HCT-116 cell lines. Both showed higher cytotoxicity against the tested cell lines compared to previously reported free ZnO (235 and 135 µg/ml for HePG-2 and HCT-116, respectively) [38].

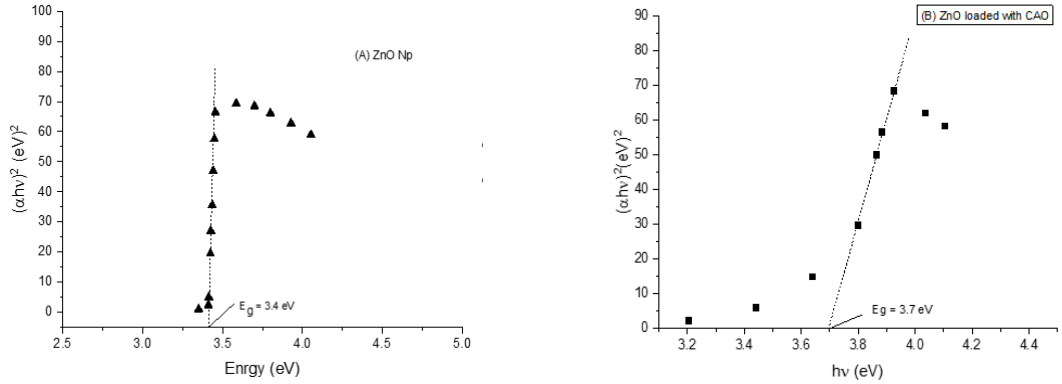

(a) **(b)**

Figure 7. The optical band gap of **(a)** ZnONPs; ZnO loaded with CAO.

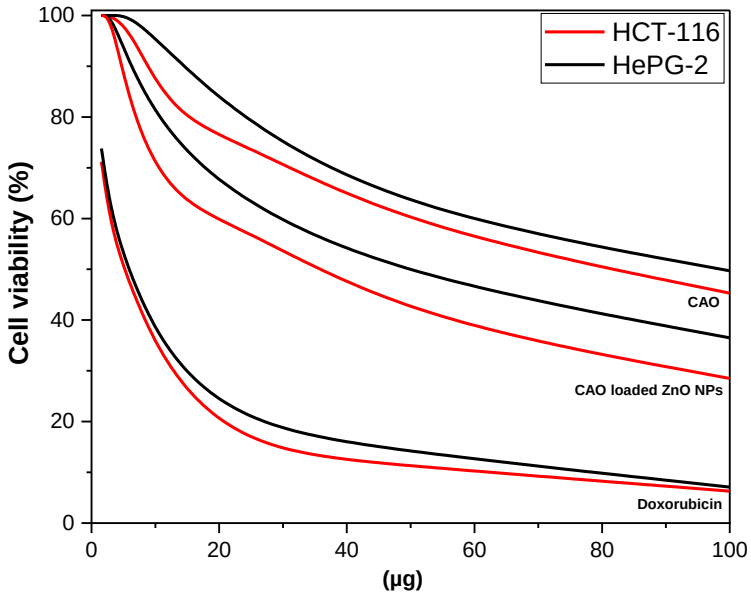

Figure 8. Percentage of cell viability after a single treatment of ZnO-loaded CAO NPs and Doxorubicin at various concentrations.

The obtained values are stated as mean ± SD, n =3. The cell viability was reduced in a dose-dependent manner after a single administration of CAO, ZnO-loaded CA, and Doxorubicin at different doses. CA and ZnO-loaded CA exhibit cytotoxicity in a dose-dependent manner on HePG-2/ HCT-116 cells, but ZnO-loaded CA is more effective than CA. The obtained results are listed in Table 1. The cell viability decreases with the higher dose of CA and ZnO-loaded CA.

Table 1. Cytotoxicity assay of the tested CA, ZnO loaded CA, and Doxorubicin on different cancer cell lines.

Compound	In vitro cytotoxicity IC_{50} (µg/mL)	
	HePG-2	HCT-116
Doxorubicin	4.50±0.2	5.23±0.3
ZnO loaded CAO NPs	47.79±2.7	32.56±2.3
CAO	74.79±3.8	87.36±4.2

It is clear that ZnO-loaded CAO shows moderate cytotoxic activity against HePG-2 and HCT-116 cells as compared with Doxorubicin (47.79±2.7µg/mL and 32.56±2.3 µg/mL Vs 4.50±0.2 µg/mL and 5.23±0.3 µg/mL) respectively, while CA showed a less cytotoxic effect as compared with Doxorubicin and ZnO loaded CA**.**

3.6. Antioxidant activity.

The antioxidant activity of ZnO-loaded CA NPs and CA (Table 2) reveals a significant DPPH free radical scavenging activity from 18.1 % to 78.2 % and from 11.9 % to 64.7 % with IC_{50} value 44.82±0.23 µg/mL and 65.99±0.39 µg/mL respectively, compared with 94.5% inhibition offered by ascorbic acid (a positive control) at 16.81±0.10µg/mL.

Table 2. Antioxidant activity of the tested CA, CA loaded ZnO NPs.

Compound	**Conc (µg/mL)**						
	10	**20**	**40**	**60**	**80**	**100**	**IC_{50}**
	% Inhibition						
Ascorbic acid	38.7	52.1	69.6	81.8	87.4	94.5	16.81±0.10
ZnO NPs loaded CAO	18.1	30.8	43.0	51.9	67.1	78.2	44.82±0.23
CAO	11.9	23.5	31.9	44.6	56.5	64.7	65.99±0.39

The results illustrate that ZnO-loaded CA NPs, and CA are able to scavenge the free radicals, and they showed higher anti-oxidant activity than previously reported free ZnO [46] in a dose-dependent manner. The antioxidant activity is higher at various concentrations of ZnO-loaded CA than at the free CA. This increment is due to the charge density of the metal ion and the increased ability of the capping materials on their surface after coordination with ZnO. The antioxidant activity was assessed by IC_{50} value, where the IC_{50} value defines the amount of the sample required to scavenge 50% of the free radicals. The best antioxidant potential is associated with the lower IC_{50} value of ZnO-loaded CA. ZnO-loaded CA and the free CA show IC_{50} values moderately higher than the standard ascorbic acid. Consequently, the results indicate that the antioxidant potency of ZnO-loaded CA and CA is lower than the standard ascorbic acid.

4. Conclusions

ZnONPs were synthesized and loaded with *Citrus aurantium* oil (CA). Different physicochemical techniques were employed to characterize ZnO loaded with CA. X-ray indicated the formation of quantum dots ZnO. The cytotoxicity and antioxidant activities of CA and ZnO-loaded CA have been studied. The results indicated that ZnO-loaded with CA has higher activity than CA alone, as the loaded compound has a dual activity for both ZnO and CA. Applying ZnO as a drug carrier of anticancer natural products is expected to be a promising, safe candidate for cancer therapy. ZnO-loaded with CA will be subjected to in vivo study to exhibit more details on its anticancer activity. Loading *Citrus aurantium* onto another biologically active metal oxide will be the point of future work.

Funding

This research received no external funding.

Conflicts of Interest

The authors declare no conflict of interest.

References

1. Bray, F.; Laversanne, M.; Weiderpass, E.; Soerjomataram, I. The ever-increasing importance of cancer as a leading cause of premature death worldwide. *Cancer* **2021**, *127*, 3029-3030, https://doi.org/10.1002/cncr.33587.
2. Anand, U.; Dey, A.; Chandel, A.K.S.; Sanyal, R.; Mishra, A.; Pandey, D.K.; De Falco, V.; Upadhyay, A.; Kandimalla, R.; Chaudhary, A.; Dhanjal, J.K.; Dewanjee, S.; Vallamkondu, J.; Pérez de la Lastra, J.M. Cancer chemotherapy and beyond: Current status, drug candidates, associated risks and progress in targeted therapeutics. *Genes Dis.* **2023**, *10*, 1367-1401, https://doi.org/10.1016/j.gendis.2022.02.007.
3. Ghosh, N.; Chatterjee, S.; Sil, P.C. Chapter1.1 - Evolution of antioxidants over times (including current global market and trend). In Antioxidants Effects in Health, Nabavi, S.M., Silva, A.S., Eds.; Elsevier, **2022**; 3-32, https://doi.org/10.1016/B978-0-12-819096-8.00011-2.
4. Mandal, A.K.; Katuwal, S.; Tettey, F.; Gupta, A.; Bhattarai, S.; Jaisi, S.; Bhandari, D.P.; Shah, A.K.; Bhattarai, N.; Parajuli, N. Current Research on Zinc Oxide Nanoparticles: Synthesis, Characterization, and Biomedical Applications. *Nanomaterials* **2022**, *12*, 3066, https://doi.org/10.3390/nano12173066.
5. Abd-Elmaqsoud, I.G.; Elsaadawi, H.A.; Ahmed, A.I.; AbdelKhalek, A.; Arisha, A. The Vast Biomedical Applications of Zinc Oxide Nanoparticles. *Zagazig Vet. J.* **2022**, *50*, 201-218, https://doi.org/10.21608/zvjz.2022.144910.1182.
6. Jha, S.; Rani, R.; Singh, S. Biogenic Zinc Oxide Nanoparticles and Their Biomedical Applications: A Review. *J. Inorg. Organomet. Polym.* **2023**, *33*, 1437–1452, https://doi.org/10.1007/s10904-023-02550-x.
7. El-Gendy, A.O.; Nawaf, K.T.; Ahmed, E.; Samir, A.; Hamblin, M.R.; Hassan, M.; Mohamed, T. Preparation of zinc oxide nanoparticles using laser-ablation technique: Retinal epithelial cell (ARPE-19) biocompatibility and antimicrobial activity when activated with femtosecond laser. *J. Photochem. Photobiol. B: Biol.* **2022**, *234*, 112540, https://doi.org/10.1016/j.jphotobiol.2022.112540.
8. Anjum, S.; Hashim, M.; Malik, S.A.; Khan, M.; Lorenzo, J.M.; Abbasi, B.H.; Hano, C. Recent Advances in Zinc Oxide Nanoparticles (ZnO NPs) for Cancer Diagnosis, Target Drug Delivery, and Treatment. *Cancers* **2021**, *13*, 4570, https://doi.org/10.3390/cancers13184570.
9. Islam, F.; Shohag, S.; Uddin, M.J.; Islam, M.R.; Nafady, M.H.; Akter, A.; Mitra, S.; Roy, A.; Emran, T.B.; Cavalu, S. Exploring the Journey of Zinc Oxide Nanoparticles (ZnO-NPs) toward Biomedical Applications. *Materials* **2022**, *15*, 2160, https://doi.org/10.3390/ma15062160.
10. Shafiee, P.; Reisi Nafchi, M.; Eskandarinezhad, S.; Mahmoudi, S.; Ahmadi, E. Sol-gel zinc oxide nanoparticles: advances in synthesis and applications. *Synth. Sinter.* **2021**, *1*, 242-254, https://doi.org/10.53063/synsint.2021.1477.
11. Wiesmann, N.; Tremel, W.; Brieger, J. Zinc oxide nanoparticles for therapeutic purposes in cancer medicine. *J. Mater. Chem. B* **2020**, *8*, 4973-4989, https://doi.org/10.1039/D0TB00739K.
12. Saravanadevi, K.; Kavitha, M.; Karpagavinayagam, P.; Saminathan, K.; Vedhi, C. Biosynthesis of ZnO and Ag doped ZnO nanoparticles from *Vitis vinifera* leaf for antibacterial, photocatalytic application. *Mater. Today: Proc.* **2022**, *48*, 352-356, https://doi.org/10.1016/j.matpr.2020.07.707.
13. Rayyif, S.M.I.; Mohammed, H.B.; Curuțiu, C.; Bîrcă, A.C.; Grumezescu, A.M.; Vasile, B.Ș.; Dițu, L.M.; Lazăr, V.; Chifiriuc, M.C.; Mihăescu, G.; Holban, A.M. ZnO Nanoparticles-Modified Dressings to Inhibit Wound Pathogens. *Materials* **2021**, *14*, 3084, https://doi.org/10.3390/ma14113084.
14. Kumar, A.; Verma, L.M.; Sharma, S.; Singh, N. Zinc oxide nanoparticles (ZnO NPs) stabilized by phytocellulose derived biopolymer and their bipartite interaction studies with agriculturally important microbes/*Raphanus sativus* (L.) seeds. *Ceram. Int.* **2023**, *49*, 39771-39787, https://doi.org/10.1016/j.ceramint.2023.07.179.
15. Xie, J.; Li, H.; Zhang, T.; Song, B.; Wang, X.; Gu, Z. Recent Advances in ZnO Nanomaterial-Mediated Biological Applications and Action Mechanisms. *Nanomaterials* **2023**, *13*, 1500, https://doi.org/10.3390/nano13091500.
16. Zahoor, S.; Sheraz, S.; Shams, D.F.; Rehman, G.; Nayab, S.; Shah, M.I.A.; Ateeq, M.; Shah, S.K.; Ahmad, T.; Shams, S.; Khan, W. Biosynthesis and Anti-inflammatory Activity of Zinc Oxide Nanoparticles Using

Leaf Extract of *Senecio chrysanthemoides*. *BioMed Res. Int.* **2023**, *2023*, 3280708, https://doi.org/10.1155/2023/3280708.
17. Singh, T.A.; Das, J.; Sil, P.C. Zinc oxide nanoparticles: A comprehensive review on its synthesis, anticancer and drug delivery applications as well as health risks. *Adv. Colloid Interface Sci.* **2020**, *286*, 102317, https://doi.org/10.1016/j.cis.2020.102317.
18. González, S.C.E.; Bolaina-Lorenzo, E.; Pérez-Trujillo, J.J.; Puente-Urbina, B.A.; Rodríguez-Fernández, O.; Fonseca-García, A.; Betancourt-Galindo, R. Antibacterial and anticancer activity of ZnO with different morphologies: a comparative study. *3 Biotech* **2021**, *11*, 68, https://doi.org/10.1007/s13205-020-02611-9.
19. Perera, W.P.T.D.; Dissanayake, R.K.; Ranatunga, U.I.; Hettiarachchi, N.M.; Perera, K.D.C.; Unagolla, J.M.; De Silva, R.T.; Pahalagedara, L.R. Curcumin loaded zinc oxide nanoparticles for activity-enhanced antibacterial and anticancer applications. *RSC Adv.* **2020**, *10*, 30785-30795, https://doi.org/10.1039/D0RA05755J.
20. Singh, R.; Cheng, S.; Singh, S. Oxidative stress-mediated genotoxic effect of zinc oxide nanoparticles on *Deinococcus radiodurans*. *3 Biotech* **2020**, *10*, 66, https://doi.org/10.1007/s13205-020-2054-4.
21. Rufino-Palomares, E.E.; Pérez-Jiménez, A.; García-Salguero, L.; Mokhtari, K.; Reyes-Zurita, F.J.; Peragón-Sánchez, J.; Lupiáñez, J.A. Nutraceutical Role of Polyphenols and Triterpenes Present in the Extracts of Fruits and Leaves of *Olea europaea* as Antioxidants, Anti-Infectives and Anticancer Agents on Healthy Growth. *Molecules* **2022**, *27*, 2341, https://doi.org/10.3390/molecules27072341.
22. Nidhi, P.; Rolta, R.; Kumar, V.; Dev, K.; Sourirajan, A. Synergistic potential of *Citrus aurantium* L. essential oil with antibiotics against *Candida albicans*. *J. Ethnopharmacol.* **2020**, *262*, 113135, https://doi.org/10.1016/j.jep.2020.113135.
23. Balahbib, A.; El Omari, N.; Ghchime, R.; Hakkour, M.; Sadak, A.; Bouyahya, A. Anti-Schistosomal Activity of Medicinal Plants: Mini Review. *Lett. Appl. NanoBioSci.* **2021**, *10*, 2352–2360, https://doi.org/10.33263/LIANBS103.23522360.
24. Naqvi, S.H.; Naseem, T.; Aziz, A.; Shah, G.M. Biological Activities and Characterization of Silver Nanoparticles from *Prunus Prescia* (L.) Batsch. *Lett. Appl. NanoBioSci.* **2021**, *10*, 2466-2482, https://doi.org/10.33263/LIANBS103.24662482.
25. Koncz, D.; Tóth, B.; Bahar, M.A.; Roza, O.; Csupor, D. The Safety and Efficacy of *Citrus aurantium* (Bitter Orange) Extracts and *p*-Synephrine: A Systematic Review and Meta-Analysis. *Nutrients*. **2022**, *14*, 4019, https://doi.org/10.3390/nu14194019.
26. Koh, A.H.W.; Chess-Williams, R.; Lohning, A.E. HPLC-UV-QDa analysis of *Citrus aurantium*-labelled pre-workout supplements suggest only a minority contain the plant extract. *J. Pharm. Biomed. Anal.* **2021**, *193*, 113746, https://doi.org/10.1016/j.jpba.2020.113746.
27. Yao, L.; Zhang, X.; Huang, C.; Cai, Y.; Wan, C. The Effect of *Citrus aurantium* on Non-Small-Cell Lung Cancer: A Research Based on Network and Experimental Pharmacology. *BioMed Res. Int.* **2023**, 2023, 6407588, https://doi.org/10.1155/2023/6407588.
28. Al-dulaimi, M.; Hammadi, M.; Sabah, R. Anti-cancer activity of ZnO Nanoparticles on Hep-G2 and HCT-116 cells. *Int. J. Pharm. Res.* **2020**, *12*, 356-364.
29. Denizot, F.; Lang, R. Rapid colorimetric assay for cell growth and survival: Modifications to the tetrazolium dye procedure giving improved sensitivity and reliability. *J. Immunol. Methods* **1986**, *89*, 271-277, https://doi.org/10.1016/0022-1759(86)90368-6.
30. Brand-Williams, W.; Cuvelier, M.E.; Berset, C. Use of free radical method to evaluate antioxidant activity. *LWT - Food Sci.Technol.* **1995**, *28*, 25–30, https://doi.org/10.1016/S0023-6438(95)80008-5.
31. Suresh, D.; Shobharani, R.M.; Nethravathi, P.C.; Pavan Kumar, M.A.; Nagabhushana, H.; Sharma, S.C. *Artocarpus gomezianus* aided green synthesis of ZnO nanoparticles: Luminescence, photocatalytic and antioxidant properties. *Spectrochim. Acta - A: Mol. Biomol. Spectrosc.* **2015**, *141*, 128-134, https://doi.org/10.1016/j.saa.2015.01.048.
32. Nakamoto, D.K.: *Infrared Spectra of Inorganic and Coordination Compounds.* Second Edition, John Wiley & Sons. New York, London, Sydney, Toronto, 1970. https://doi.org/10.1002/bbpc.19710750622.
33. Hosny, N.M.; Sherif, Y.E. Synthesis, optical band gap and anti-rheumatic activity of Fe_2O_3 nanocrystals via solid state decomposition of 4-aminophenol precursor. *Chem. Data Collect.* **2022**, *37*, 100813, https://doi.org/10.1016/j.cdc.2021.100813.
34. Hosny, N.M.; Hussien, M.A.; Radwan, F.M.; Nawar, N. Synthesis, spectral characterization and DNA binding of Schiff-base metal complexes derived from 2-amino-3-hydroxyprobanoic acid and acetylacetone.

Spectrochim. Acta - A: Mol. Biomol. Spectrosc. **2014**, *132*, 121-129, https://doi.org/10.1016/j.saa.2014.04.165.

35. Hosny, N.M.; Hussien, M.A.; Radwan, F.M.; Nawar, N. Synthesis, spectral, thermal and optical properties of Schiff-base complexes derived from 2(E)-2-((z)-4-hydroxypent-3-en-2-ylideneamino)-5-guanidinopentanoic acid and acetylacetone. *J. Mol. Struct.* **2017**, *1143*, 176-183, https://doi.org/10.1016/j.molstruc.2017.04.063.
36. Hosny, N.M. Synthesis, characterization, theoretical calculations and catalase-like activity of mixed ligand complexes derived from alanine and 2-acetylpyridine. *Transition Met. Chem.* **2007**, *32*, 117-124, https://doi.org/10.1007/s11243-006-0132-z.
37. Hosny, N.M.; Hassan, N.Y.; Mahmoud, H.M.; Abdel-Rhman, M.H. Synthesis, characterization and cytotoxicity of new 2-isonicotinoyl-N-phenylhydrazine-1-carbothioamide and its metal complexes. *Appl. Organomet. Chem.* **2019**, *33*, e4998, https://doi.org/10.1002/aoc.4998.
38. Nicol, A.W. X-ray Diffraction. In Physicochemical Methods of Mineral Analysis, Nicol, A.W., Ed.; Springer US, Boston, MA, **1975**; 249-320, https://doi.org/10.1007/978-1-4684-2046-3_7.
39. Kumar, S.S.; Venkateswarlu, P.; Rao, V.R.; Rao, G.N. Synthesis, characterization and optical properties of zinc oxide nanoparticles. *Int. Nano Lett.* **2013**, *3*, 30, https://doi.org/10.1186/2228-5326-3-30.
40. Zak, A.K.; Majid, W.H.A.; Darroudi, M.; Yousefi, R. Synthesis and characterization of ZnO nanoparticles prepared in gelatin media. *Mater. Lett.* **2011**, *65*, 70–73, https://doi.org/10.1016/j.matlet.2010.09.029.
41. Babapour, H.; Jalali, H.; Mohammadi Nafchi, A. The synergistic effects of zinc oxide nanoparticles and fennel essential oil on physicochemical, mechanical, and antibacterial properties of potato starch films. *Food Sci. Nutr.* **2021**, *9*, 3893-3905, https://doi.org/10.1002/fsn3.2371.
42. Sahai, A.; Goswami, N. Probing the dominance of interstitial oxygen defects in ZnO nanoparticles through structural and optical characterizations. *Ceram. Int.* **2014**, *40*, 14569–14578, https://doi.org/10.1016/j.ceramint.2014.06.041.
43. Hosny, N.M. Synthesis, characterization and optical band gap of NiO nanoparticles derived from anthranilic acid precursors via a thermal decomposition route. *Polyhedron* **2011**, *30*, 470–476, https://doi.org/10.1016/j.poly.2010.11.020.
44. Hosny, N.M.; Dahshan, A. Facile synthesis and optical band gap calculation of Mn_3O_4 nanoparticles. *Mater. Chem. Phys.* **2012**, *137*, 637-643, https://doi.org/10.1016/j.matchemphys.2012.09.068.
45. Hosny, N.M. Single crystalline Co_3O_4: Synthesis and optical properties. *Mater. Chem. Phys.* **2014**, *144*, 247-251, https://doi.org/10.1016/j.matchemphys.2013.12.022.
46. Nagajyothi, P.C.; Cha, S.J.; Yang, I.J.; Sreekanth, T.V.M.; Kim, K.J.; Shin, H.M. Antioxidant and anti-inflammatory activities of zinc oxide nanoparticles synthesized using *Polygala tenuifolia* root extract. *J. Photochem. Photobiol. B.* **2015**, *146*, 10-17, https://doi.org/10.1016/j.jphotobiol.2015.02.008.